X Entanglement: The Nonfactorable Spatiotemporal Structure of Biphoton Correlation

A. Gatti, E. Brambilla, L. Caspani, O. Jedrkiewicz, and L. A. Lugiato

INFM-CNR-CNISM, Dipartimento di Fisica e Matematica, Università dell'Insubria, Via Valleggio 11, 22100 Como, Italy

(Received 16 December 2008; published 4 June 2009)

We investigate the spatiotemporal structure of the biphoton entanglement in parametric down-conversion (PDC) and we demonstrate its nonfactorable X-shaped geometry. Such a structure gives access to the ultrabroad bandwidth of PDC, and can be exploited to achieve a biphoton temporal localization in the femtosecond range. This extreme localization is connected to our ability to resolve the photon positions in the source near field. The nonfactorability opens the possibility of tailoring the temporal entanglement by acting on the spatial degrees of freedom of twin photons.

DOI: 10.1103/PhysRevLett.102.223601 PACS numbers: 42.50.Dv, 42.50.Ar

Parametric down-conversion (PDC) is probably the most efficient and widely used source of entangled photon pairs which have been employed in several successful implementations of quantum communication and information schemes. At the very heart of such technologies lies the quantum interference between photonic wave functions, which depends crucially on the spatiotemporal mode structure of the photons. In this work, the issue of controlling and tailoring the biphoton spatiotemporal structure is addressed from a peculiar and novel point of view, that is, the nonfactorability in space and time of the PDC biphoton entanglement. The idea comes from the context of nonlinear optics, where recent studies [1] outlined how in nonlinear media the angular dispersion relations impose a hyperbolic geometry involving both temporal and spatial degrees of freedom in a nonfactorable way. The wave object that captures such a geometry is the so-called X wave, which is a localized and propagation-invariant wave packet, nonseparable in space and time. The statistical counterpart of the X wave was shown [2] to emerge in the X-shaped structure of the coherence function, describing the classical phase coherence of the individual signal (idler) field.

In this Letter, we turn our attention to the genuine quantum level, investigating the spatiotemporal structure of the biphoton cross correlation, the quantity that is at the heart of the photon-pair PDC entanglement. We shall demonstrate that an X geometry emerges in this microscopic context as well. With few exceptions [3,4], the PDC entanglement has been, to date, investigated mostly either in a purely temporal [5–7] or spatial [8–10] framework. Our approach, based on the nonfactorability in space and time of the state, will point out a key element of novelty, i.e., the possibility of tailoring the temporal bandwidth of the biphotons by manipulating their spatial degrees of freedom. In particular, by resolving their near-field positions, we will show that the X structure opens the access to an ultrabroad bandwidth entangled photonic source, with a temporal localization in the femtosecond range. Such an extreme localization can be used to increase the sensitivity of high-precision measurements, e.g., in the protocol of clock synchronization [11] or of quantum optical coherence tomography [12]. Our results compare with recent findings [13], where a $\sim$7 fs Hong-Ou-Mandel dip was observed through the use of a quasi-phase-matched nonlinear grating.

We shall focus on type I PDC, in the low-gain (coincidence count) regime. We remark that the X structure of entanglement is a general feature of PDC, present also in type II and in the high-gain regime [14]. The model is basically the same as in [4,10]. A quasimonochromatic and coherent pump field propagates along the direction z inside a slab of nonlinear $\chi^{(2)}$ crystal of length l_c. $\hat{A}_p(\mathbf{x}, t, z)$, $\hat{A}_s(\mathbf{x}, t, z)$ denote the envelope operators of the pump and the down-converted signal field of central frequencies ω_p and $\omega_s = \omega_p/2$, respectively. Here $\mathbf{x} = (x, y)$ labels the transverse coordinates, while t is time. We next pass to the Fourier domain: $\hat{A}_i(\mathbf{q}, \omega, z) = \int \frac{d^2\mathbf{x}}{2\pi} \times \int \frac{dt}{\sqrt{2\pi}} \hat{A}_i(\mathbf{x}, t, z) e^{-i\mathbf{q}\cdot\mathbf{x}+i\omega t}$, $i = s, p$, and extract the fast variation due to their linear propagation along the crystal slab:

$$\hat{A}_i(\mathbf{q}, \omega, z) = e^{ik_{iz}(\mathbf{q},\omega)z} \hat{a}_i(\mathbf{q}, \omega, z), \qquad i = s, p, \tag{1}$$

where $k_{iz}(\mathbf{q}, \omega) = \sqrt{k_i^2(\mathbf{q}, \omega) - q^2}$ is the z component of the wave vector of the ith field, $k_i(\mathbf{q}, \omega)$ being the wave number at frequency ω, which depends on the transverse wave vector $\mathbf{q}$ only for the extraordinary wave. The fields $\hat{a}_i$ defined in this way have a slow variation along the crystal, arising only from the nonlinear interaction. In the low-gain regime we can assume that the pump is undepleted by the nonlinear interaction [$\frac{d}{dz}\hat{a}_p(\mathbf{q}, \omega, z) = 0$] and substitute its field operator by a c-number field $\alpha_p(\mathbf{q}, \omega)$, so that the pump evolution along the crystal is described by $\mathcal{A}_p(\mathbf{q}, \omega, z) = e^{ik_{pz}(\mathbf{q},\omega)z}\alpha_p(\mathbf{q}, \omega)$. For the signal field, its propagation along the crystal is described by [4]

$$\frac{\partial \hat{a}_s(\mathbf{q}, \omega, z)}{\partial z} = \frac{g}{l_c} \int \frac{d^2\mathbf{q}'}{2\pi} \int \frac{d\omega'}{\sqrt{2\pi}} [\alpha_p(\mathbf{q} + \mathbf{q}', \omega + \omega') \times \hat{a}_s^\dagger(\mathbf{q}', \omega', z) e^{-i\Delta(\mathbf{q},\omega,\mathbf{q}',\omega')z}], \tag{2}$$

where g is the dimensionless parametric gain, proportional to the second-order $\chi^{(2)}$ susceptibility, to the crystal length l_c and to the pump peak value (the pump field has been normalized to its peak value). The phase-mismatch function

$$\Delta(\mathbf{q}, \omega, \mathbf{q}', \omega') = k_{sz}(\mathbf{q}, \omega) + k_{sz}(\mathbf{q}', \omega') - k_{pz}(\mathbf{q} + \mathbf{q}', \omega + \omega') \tag{3}$$

determines how efficiently a pump photon with transverse wave vector $\mathbf{q} + \mathbf{q}'$ and frequency $\omega_p + \omega + \omega'$ is down-converted into a pair of photons with transverse wave vectors $\mathbf{q}$, $\mathbf{q}'$ and frequencies $\omega_s + \omega$, $\omega_s + \omega'$: the smaller its modulus, the higher the probability that such an elementary process occurs.

In most experiments in the low-gain regime, the quantity of primary interest is the two-photon correlation, also called biphoton amplitude. We shall study this quantity in the spatiotemporal domain, in a plane at the output face of the crystal (near-field plane); that is, we focus on

$$\psi(\mathbf{x}, t, \mathbf{x}', t') = \langle \hat{A}_s(\mathbf{x}, t, l_c) \hat{A}_s(\mathbf{x}', t', l_c) \rangle. \tag{4}$$

In the low-gain limit its square modulus $|\psi(\mathbf{x}, t, \mathbf{x}', t')|^2$ is proportional to the two-photon coincidence rate $G^{(2)}(\mathbf{x}, t, \mathbf{x}', t')$, which gives the joint probability distribution of finding two photons in position $\mathbf{x}$ at time t and position $\mathbf{x}'$ at time t', respectively.

For small gains ($g \ll 1$), the propagation equation (2) can be solved perturbatively up to first order in g, obtaining the following expression for the biphoton amplitude in the Fourier domain:

$$\begin{aligned} &\langle \hat{A}_s(\mathbf{q}_1, \omega_1, l_c) \hat{A}_s(\mathbf{q}_2, \omega_2, l_c) \rangle \\ &= (2\pi)^{-3/2} g \mathcal{A}_p(\mathbf{q}_1 + \mathbf{q}_2, \omega_1 + \omega_2, l_c) \\ &\quad \times e^{i\Delta(\mathbf{q}_1, \omega_1, \mathbf{q}_2, \omega_2) l_c/2} \operatorname{sinc}\left[\frac{\Delta(\mathbf{q}_1, \omega_1, \mathbf{q}_2, \omega_2) l_c}{2}\right]. \end{aligned} \tag{5}$$

In the literature the same quantity is usually derived through a perturbative evaluation of the two-photon state vector (see, e.g., [3]).

In order to simplify our results, we consider the limit of a nearly plane wave and monochromatic pump, i.e., a pump of waist w_p and duration τ_p large enough, so that the dependence of the phase mismatch Δ on $\mathbf{q}_1 + \mathbf{q}_2$ and $\omega_1 + \omega_2$ (the pump variables) can be neglected. It can be shown [14] that such an approximation holds when w_p and τ_p are much larger than the spatial walk-off and the temporal delay due to group velocity mismatch, respectively, experienced by the signal and the pump after crossing the crystal. Typical values are ~ 300 μm and ~ 2 ps, as in the example of a 4 mm β-barium-borate (BBO) crystal cut for degenerate type I PDC at 352 nm. Provided that such conditions hold, the biphoton amplitude (4) at the crystal output takes the factorized form

$$\psi(\mathbf{x}, t, \mathbf{x}', t') = \mathcal{A}_p\left(\frac{\mathbf{x} + \mathbf{x}'}{2}, \frac{t + t'}{2}, l_c\right) \psi_{\mathrm{pw}}(\mathbf{x} - \mathbf{x}', t - t'), \tag{6}$$

where

$$\psi_{\mathrm{pw}}(\boldsymbol{\xi}, \tau) = \int \frac{d^2\mathbf{q}}{(2\pi)^2} \int \frac{d\omega}{2\pi} e^{i\mathbf{q}\cdot\boldsymbol{\xi} - i\omega\tau} V(\mathbf{q}, \omega) \tag{7a}$$

$$V(\mathbf{q}, \omega) = g e^{i\Delta_{\mathrm{pw}}(\mathbf{q}, \omega) l_c/2} \operatorname{sinc}\left[\frac{\Delta_{\mathrm{pw}}(\mathbf{q}, \omega) l_c}{2}\right], \tag{7b}$$

$$\Delta_{\mathrm{pw}}(\mathbf{q}, \omega) = k_{sz}(\mathbf{q}, \omega) + k_{sz}(-\mathbf{q}, -\omega) - k_p(0, 0) \tag{7c}$$

is the plane-wave pump result for the field correlation function. The pump beam profile $\mathcal{A}_p$ acts thus as a slow modulation over the plane-wave pump correlation ψ_{pw} that depends only on the relative coordinates $\boldsymbol{\xi} = \mathbf{x} - \mathbf{x}'$, $\tau = t - t'$, as it can be expected in the nearly stationary and homogeneous conditions considered here.

A first qualitative insight into the problem can be obtained by considering the usual quadratic expansion of the phase-matching function, equivalent to adopting the paraxial and quadratic dispersion approximations. In the case of *e-oo* phase matching, it takes the form [4]:

$$\Delta_{\mathrm{pw}}(\mathbf{q}, \omega) l_c \approx \Delta_0 + \frac{\omega^2}{\Omega_0^2} - \frac{q^2}{q_0^2}, \tag{8}$$

where $\Delta_0 = (2k_s - k_p) l_c$ is the collinear phase mismatch at degeneracy, $\Omega_0 = \sqrt{1/k_s'' l_c}$, $q_0 = \sqrt{k_s/l_c}$, and we used the shorthand notation $k_s = k_s(0, 0)$, $k_p = k_p(0, 0)$, $k_s'' = d^2 k_s/d\omega^2|_{0,0}$. If we extend the validity of such an approximation to the entire $(\mathbf{q}, \omega)$ domain, and we use the identity $e^{ip/2} \operatorname{sinc}(p/2) = \int_0^1 ds e^{isp}$, the biphoton amplitude $\psi_{\mathrm{pw}}(\boldsymbol{\xi}, \tau)$ can be recast in the integral form:

$$\psi_{\mathrm{pw}}(r, \tau) = g \frac{q_0^2 \Omega_0}{8\sqrt{\pi^3 i}} \int_0^1 \frac{ds}{s^{3/2}} e^{(i/4s)(q_0^2 r^2 - \Omega_0^2 \tau^2)} e^{is\Delta_0}, \tag{9}$$

where $r = |\boldsymbol{\xi}|$ indicates the radial coordinate. This expression clearly evidences the hyperbolic geometry of $\psi_{\mathrm{pw}}(r, \tau)$: the function is indeed constant on the rotational hyperboloids where the argument

$$H(r, \tau) \equiv q_0^2 r^2 - \Omega_0^2 \tau^2 \tag{10}$$

assumes constant values. However, it can be easily shown that $\psi_{\mathrm{pw}}(H)$ goes as $1/\sqrt{|H|}$ for $|H| \to 0$, that is, when approaching the asymptotes of the X structure, where $H(r, \tau) = q_0^2 r^2 - \Omega_0^2 \tau^2 = 0$. This singularity arises from the unphysical assumption that the approximation (8) is valid everywhere.

In order to obtain quantitative results we need therefore to go beyond the paraxial and quadratic dispersion approximations in the evaluation of $\Delta(\mathbf{q}, \omega)$ and drop the approximation (8). $\psi_{\mathrm{pw}}(\boldsymbol{\xi}, \tau)$, defined by Eq. (7), is hence numerically calculated by using the complete Sellmeier relations [15] for the refractive indexes. An example of our results is shown by Fig. 1 for the case of a type I BBO crystal. Since the signal is an ordinary wave, the spatial radial symmetry

of the problem can be exploited to compute Eq. (7) by means of a Fourier-Hankel transform. Correspondingly, the biphoton amplitude $\psi_{\rm pw}$ depends only on the radial coordinate $|\boldsymbol{\xi}|$. A cut of this function in the (ξ_x, τ) plane is displayed in Figs. 1(a) and 1(b) (the whole three-dimensional plot has a radial symmetry in space, and shows a biconical geometry). A clear X-shaped structure emerges: this nontrivial shape of the spatiotemporal two-photon correlation, that we shall call X *entanglement*, can be considered the counterpart, at the quantum level, of the nonlinear X waves [1]. Similar results hold for a variety of phase-matching conditions and crystal lengths [14].

A remarkable characteristic of the X entanglement is the unusually small width of the spatiotemporal correlation peak, which corresponds to a strong relative localization of twin photons both in time and space. The two lower frames of Fig. 1 plot cuts of the two-photon coincidence rate $|\psi_{\rm pw}|^2$ along the temporal and spatial axis, respectively. The relative spatial localization is remarkable but not impressive, as displayed in Fig. 1(d) by the $\tau = 0$ spatial profile, which has a FWHM of $\sim$2.9 μm. More impressive, and, in a sense, unexpected, is the relative localization in time of twin photons, which can be appreciated from the temporal profile $|\psi_{\rm pw}(\mathbf{0}, \tau)|^2$ in Fig. 1(c), which is as narrow as 4.4 fs. Such an ultrashort two-photon localization emerges spontaneously from a nearly monochromatic pump, as a consequence of the ultrabroad bandwidth of PDC phase matching, which in principle extends over the optical frequency $\omega_p \sim 5 \times 10^{15}$ Hz. Notice that,

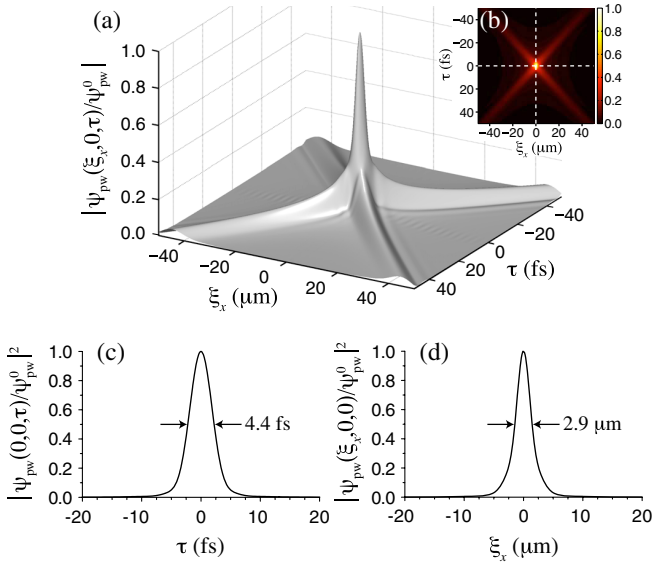

FIG. 1 (color online). (a),(b) 2D cut of the biphoton amplitude at $\xi_y = 0$, clearly displaying its X-shaped geometry (the whole 3D plot has a biconical shape). (c),(d) 1D cuts of the coincidence rate $|\psi_{\rm pw}|^2$ along the temporal (c) and spatial (d) coordinate axis [indicated by the two dashed lines in (b)]. The width of the peaks shows the relative temporal and spatial localization of biphotons. $\psi^0_{\rm pw} = \psi_{\rm pw}(\mathbf{0}, 0)$. BBO crystal, cut at 33.436°; $g = 10^{-3}$, $\lambda_p = 352$ nm, $l_c = 4$ mm.

in order to account for, e.g., the finite bandwidth of detection, in our calculations we include a super-Gaussian frequency filter centered at degeneracy. The 4.4 fs width of the temporal peak is in practice determined by the width of this frequency filter (see Fig. 2 for a comparative view of the bandwidths involved).

It is interesting to compare our results with the typical $\sim$100 fs temporal localization of the coincidence rate measured in the far-field zone, by collecting twin photons that propagate at symmetric directions $\mathbf{q}$ and $-\mathbf{q}$, within a small angular bandwidth. In that case, the measured quantity is proportional to $|V(\mathbf{q}, \tau)|^2 = |\int \frac{d\omega}{2\pi} e^{-i\omega\tau} V(\mathbf{q}, \omega)|^2$. Its temporal width is determined by the inverse of the bandwidth of the spectrum $V(\mathbf{q}, \omega)$ at fixed q, i.e., the narrow (10^{13}–10^{14} Hz) thickness of the curve in Fig. 2. This bandwidth can be roughly evaluated as Ω_0 for $q/q_0 \ll 1$, and as $\Omega_0 q_0/q$ for $q/q_0 > 1$. Clearly, since Ω_0 scales as $l_c^{-1/2}$, the shorter the crystal, the stronger the temporal localization in the far field; however, a far-field localization in the femtosecond range would require a crystal as short as $\sim$50 μm, with a strongly reduced down-conversion efficiency. Conversely, in our case, the detection of coincidences in the near field gives in principle access to the full ($\sim 10^{15}$ Hz) bandwidth of phase matching even for a long crystal.

It is, however, important to stress that such an extreme temporal localization of twin photons relies on the ability to resolve their relative position in the near-field plane. Indeed, a measurement collecting all the photons over the beam cross section, without discriminating their positions, is characterized by the integrated coincidence rate $\int d^2\boldsymbol{\xi} |\psi_{\rm pw}(\boldsymbol{\xi}, \tau)|^2$, reproduced by the dashed curve in Fig. 3, which has a width of $\sim$100 fs. This may appear surprising because in this measurement all the photons at the different frequencies within the phase matching are collected. However, the identity $\int d^2\boldsymbol{\xi} |\psi_{\rm pw}(\boldsymbol{\xi}, \tau)|^2 = \int d^2\mathbf{q} |V(\mathbf{q}, \tau)|^2$ shows that in this case the coincidence rate takes the form of an incoherent superposition of the

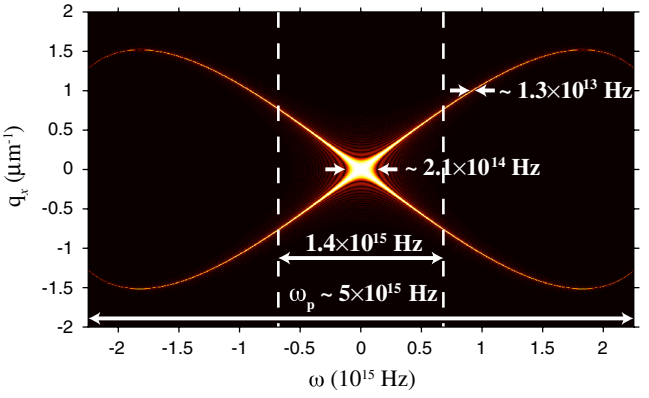

FIG. 2 (color online). Plot of $|V|$ showing the phase-matching curve in the (q_x, ω) plane. The dashed lines show the bandwidth selected by the filter, and the arrows indicate the different bandwidths involved (same parameters as in Fig. 1).

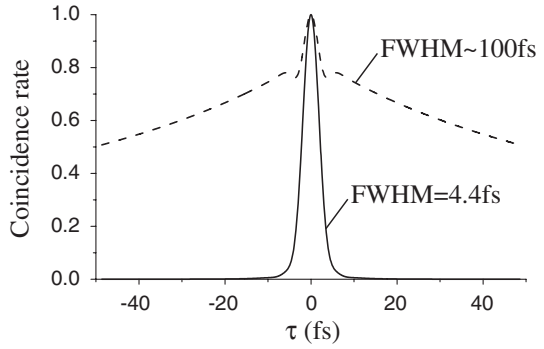

FIG. 3. Solid line: $|\psi_{\mathrm{pw}}(\boldsymbol{\xi}=\mathbf{0},\tau)|^2$, coincidence rate when twin photons are collected at the same near-field position. Dashed line: $\int d^2\boldsymbol{\xi}|\psi_{\mathrm{pw}}(\boldsymbol{\xi},\tau)|^2$, coincidence rate measured without resolving photon positions.

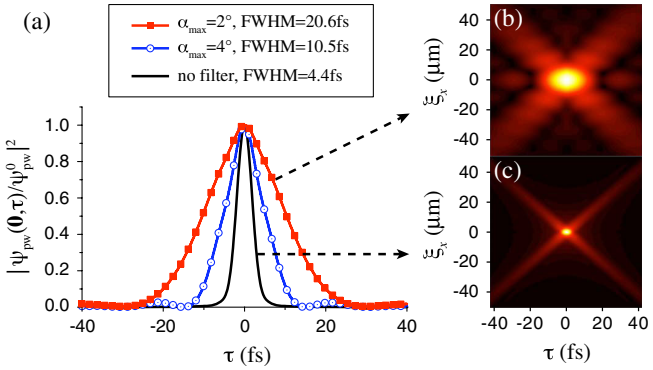

FIG. 4 (color online). Effect of spatial filtering on the X entanglement. (a) Temporal correlation peak $|\psi_{\mathrm{pw}}(\mathbf{0},\tau)|^2$ in the presence of a spatial filter, that cuts the angular spectrum at an angle $\alpha_{\max}$. The two insets show the full X correlation for $\alpha_{\max}=2^0$ (b) and in the absence of the spatial filter (c).

probabilities of detecting a pair of photons at a given q and has therefore the same $\sim$100 fs temporal localization as the far-field coincidence rate at fixed q. Conversely, by resolving the near-field positions of twin photons, the measured quantity is $|\psi_{\mathrm{pw}}(\mathbf{0},\tau)|^2=|\int\frac{d^2\mathbf{q}}{(2\pi)^2}V(\mathbf{q},\tau)|^2$, which is a coherent superposition of the probability amplitudes at a given q (i.e., at a given frequency due to the angle-frequency relation imposed by phase matching), and therefore allows a stronger temporal localization.

The nonfactorability in space and time of the X entanglement thus opens the relevant possibility of tailoring the temporal bandwidth of the biphotons by acting on their spatial degrees of freedom. As a specific example, let us consider the effects of spatial filtering on the temporal correlation. Let us assume that a $4f$ lens system is employed to image the near field of the PDC fluorescence, and that a circular aperture of radius r_a is located in the far-field $2f$ plane, acting as a filter that cuts all the angular spectrum at $\alpha>\alpha_{\max}=\arcsin(r_a/f)$. Figure 4 shows the effect on the temporal correlation peak. While in the absence of any spatial filter the correlation shows a strong temporal localization, as the angular bandwidth is reduced by spatial filtering, the two-photon correlation broadens in time, which gives clear evidence of the nonfactorability of the correlation.

In conclusion, this work demonstrates that the X geometry is intrinsic to PDC at the microscopic quantum level of photon-pair entanglement. As for the macroscopic X waves and the classical phase coherence of PDC [2], the nonfactorability is imposed by the phase-matching mechanism governing the wave-mixing processes. Following this analogy, we coined the name of X entanglement. The key element of novelty that emerges in the microscopic context is the extreme relative localization of twin photons, with correlation times and correlation lengths in the femtosecond and micrometer range, respectively. The strong temporal localization is determined by the full extent of the PDC bandwidth, rather than by the bandwidth $\sim\Omega_0$ characterizing the PDC far field. For this reason, a near-field measurement scheme able to resolve spatially the coincidences would provide a powerful tool for high-precision measurements, capable of improving substantially the resolution power in the temporal domain with respect to standard schemes.

We thank P. Di Trapani and M. Clerici for useful discussions. Work supported by the FET programme of the EC, under the GA HIDEAS FP7-ICT-221906.

[1] For a review, see C. Conti, P. Di Trapani, and S. Trillo, in *Self-focusing: Past and Present*, Topics in Applied Physics Vol. 114, edited by R. W. Boyd, S. G. Lukishova, Y. R. Shen (Springer, New York, 2009).
[2] O. Jedrkiewicz *et al.*, Phys. Rev. Lett. **97**, 243903 (2006); Phys. Rev. A **76**, 033823 (2007).
[3] M. Atatüre *et al.*, Phys. Rev. A **65**, 023808 (2002).
[4] A. Gatti, R. Zambrini, M. San Miguel, and L. A. Lugiato, Phys. Rev. A **68**, 053807 (2003).
[5] C. K. Hong, Z. Y. Ou, and L. Mandel, Phys. Rev. Lett. **59**, 2044 (1987).
[6] C. K. Law, I. A. Walmsley, and J. H. Eberly, Phys. Rev. Lett. **84**, 5304 (2000).
[7] W. P. Grice, A. B. U'Ren, and I. A. Walmsley, Phys. Rev. A **64**, 063815 (2001).
[8] M. H. Rubin, Phys. Rev. A **54**, 5349 (1996).
[9] C. K. Law and J. H. Eberly, Phys. Rev. Lett. **92**, 127903 (2004).
[10] A. Gatti, E. Brambilla, and L. Lugiato, Prog. Opt. **51**, 251 (2008); E. Brambilla, A. Gatti, M. Bache, and L. A. Lugiato, Phys. Rev. A **69**, 023802 (2004).
[11] V. Giovannetti, S. Lloyd, L. Maccone, and F. N. C. Wong, Phys. Rev. Lett. **87**, 117902 (2001).
[12] A. F. Abouraddy *et al.*, Phys. Rev. A **65**, 053817 (2002).
[13] M. B. Nasr *et al.*, Phys. Rev. Lett. **100**, 183601 (2008).
[14] L. Caspani, E. Brambilla, L. Lugiato, and A. Gatti (to be published).
[15] N. Boeuf *et al.*, Opt. Eng. (Bellingham, Wash.) **39**, 1016 (2000).